Expert Systems With Applications 238 (2024) 121842

Contents lists available at ScienceDirect

Expert Systems With Applications

journal homepage: www.elsevier.com/locate/eswa

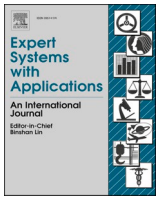

Santiago urban dataset SUD: Combination of Handheld and Mobile Laser Scanning point clouds

Silvia María González-Collazo [a,*], Jesús Balado [a], Iván Garrido [a], Javier Grandío [a], Rabia Rashdi [a], Elisavet Tsiranidou [a], Pablo del Río-Barral [a], Erik Rúa [a], Iván Puente [b], Henrique Lorenzo [a]

[a] CINTECX, Universidade de Vigo, GeoTECH Group, 36310 Vigo, Spain
[b] Defense University Center at the Spanish Naval Academy, 36920 Marín, Spain

ARTICLE INFO

Keywords:
Deep learning
LiDAR
Semantic segmentation
Mobile mapping systems
Occlusions
Urban mobility

ABSTRACT

Santiago Urban Dataset SUD is a real dataset that combines Mobile Laser Scanning (MLS) and Handheld Mobile Laser Scanning (HMLS) point clouds. The data is composed by 2 km of streets, sited in Santiago de Compostela (Spain). Point clouds undergo a manual labelling process supported by both heuristic and Deep Learning methods, resulting in the classification of eight specific classes: *road, sidewalk, curb, buildings, vehicles, vegetation, poles*, and *others*. Three PointNet++ models were trained; the first one using MLS point clouds, the second one with HMLS point clouds and the third one with both H&MLS point clouds. In order to ascertain the quality and efficacy of each Deep Learning model, various metrics were employed, including confusion matrices, precision, recall, F1-score, and IoU. The results are consistent with other state-of-the-art works and indicate that SUD is valid for comparing point cloud semantic segmentation works. Furthermore, the survey's extensive coverage and the limited occlusions indicate the potential utility of SUD in urban mobility research.

1. Introduction

Point cloud data is increasingly used in several urban applications such as BIM (Building Information Modelling) (Romero-Jarén & Arranz, 2021), city mapping (Murtiyoso et al., 2020), road infrastructure management (Gouda et al., 2021; Justo et al., 2021), or construction of HD (High Definition) maps for autonomous driving (Gao et al., 2021; Ma et al., 2019). In addition, several studies focus their research on pedestrian urban mobility. Balado et al., (2019) presented a methodology for the use of point clouds for direct pathfinding in urban environments. Fernández-Arango et al., (2022) characterized the urban space available for walking, by segmenting Mobile Laser Scanning (MLS) point clouds. Ito & Takemura, (2021) proposed a method to estimate the mobility of intelligent electric wheelchairs users using eye movements and point clouds. Soilán et al., (2018) presented an automatic methodology for the assessment of several safety indicators in urban crosswalks. In many of urban applications the detection and classification of the point cloud objects is needed (Fernandes et al., 2021). Recently, the use of Deep Learning methods has become the state of the art in point cloud classification (Kim et al., 2020; Ma et al., 2020; Zou et al., 2017) which deals with the need for large labelled datasets to train the Neural Networks.

Traditional laser scanning systems include Terrestrial Laser Scanning (TLS), Mobile Laser Scanning (MLS) and Aerial Laser Scanning (ALS), although new types of platforms are in the market, as Handheld Mobile Laser Scanning (HMLS) or UAV Laser Scanning (ULS) (Soilán et al., 2019). Through all these possibilities, both outdoor and indoor spaces can be digitalized. For indoor spaces, TLS or HMLS are preferably employed. For outdoor spaces, the selection of the laser scanning systems depends on the purpose and the laser scanning mobility. MLS obtains a large amount of information in a short time, e.g., scanning kilometres of roads. However, MLS data usually features numerous sidewalk occlusions, mainly occurred by parked vehicles (Barros-Ribademar et al., 2022). These occlusions imply a lack of knowledge of the pedestrian urban environment and, although several methods have been proposed for their systematic regeneration, (Liu et al., 2022),these methods do not necessarily coincide with reality as they do not consider the existence of sidewalk surface damages or hidden objects, barriers of pedestrian mobility. Therefore, despite the existence of point cloud urban datasets to train Neural Networks, these datasets contain unreal or incomplete data of the pedestrian urban environment.

* Corresponding author.
E-mail address: silvgonzalez@uvigo.es (S.M. González-Collazo).

https://doi.org/10.1016/j.eswa.2023.121842
Received 16 June 2023; Received in revised form 22 August 2023; Accepted 25 September 2023
Available online 2 October 2023

This paper presents a large labelled point cloud database acquired in Santiago de Compostela (Spain). The Santiago Urban Dataset (SUD) was acquired with MLS and HMLS. Both data were georeferenced and labelled into eight main classes: *road*, *sidewalk*, *curb*, *buildings*, *vehicles*, *vegetation*, *pole-like elements* and *others*. The novelty of this research is to provide a complete dataset with real pedestrian urban environment, which distinguishes the ground urban elements. By combining MLS with HMLS data, occlusions in sidewalks are removed, and the dataset becomes highly suitable for pedestrian mobility studies and a valuable resource for training Deep Learning models.

This paper is organized as follows: Section 2 collects the related work of urban point cloud datasets. Section 3 presents the data generation. In Section 4, the results obtained are shown. Section 5 is devoted to the discussion. Finally, Section 6 presents the conclusions.

2. Related work

The increased use of LiDAR sensors and cameras favours a rise in 3D point cloud datasets, while the increased use of Deep Learning (Bello et al., 2020; Guo et al., 2021) contributes to the need for labelled databases. These 3D point cloud datasets can be obtained synthetically (Griffiths & Boehm, 2019) or can be scanned with different sensors and in different spaces, regarding indoor and outdoor spaces. Furthermore, open access data contributes to a wider dissemination and sharing of results.

Although there are also several indoor datasets (Chang et al., 2017; Dai et al., 2017), most point cloud datasets were taken in outdoor scenes. Regarding to urban environments, MLS offers the advantage of scanning many road metres in a short time. However, occlusions appear in MLS point clouds mainly due to parked vehicles (Barros-Ribademar et al., 2022), making MLS point clouds difficult to be useful for studying pedestrian mobility. (Balado et al., 2019) presented a method for pedestrian pathfinding from point clouds and they had to correct occlusions with morphological operations. The proposed SUD dataset eliminates occlusions by combining both MLS and HMLS data. With the HMLS data, most of the sidewalk points are obtained, filling in the MLS occlusions without resorting to synthetic data that may not match reality.

Most datasets focus the attention on labelling the ground, vegetation, buildings and pole-like elements or tree trunks. In Toronto-3D (Tan et al., 2020) e.g., all ground is considered as class *road*. Some datasets made a more detailed classification of the ground. In TUM-MLS-2016 (Zhu et al., 2020), only a distinction is made between *man-made* and *natural terrain*. The Synthcity dataset (Griffiths & Boehm, 2019), composed by synthetic point clouds, split the ground points into *road* and *pavement*. The Paris-Lille-3D dataset (Roynard et al., 2018) includes more than 50 classes, considering buildings, vehicles, vegetation and poles among others, and the ground is classified into *road* and *sidewalk*. Both datasets distinguish between sidewalk and road, however curbs are not considered, being one of the main barriers for people with reduced mobility. In the SUD dataset, the ground is also labelled in more detail, considering *sidewalk* (occlusion-free), *road* and *curbs*. Other classes relevant to urban mobility such as *buildings*, *vehicles*, *vegetation*, and *poles* are also labelled.

Some datasets present synthetic point clouds or a combination of synthetic and real point clouds, e.g. Paris-CARLA-3D (Deschaud et al., 2021). One of the primary benefits of a self-constructed synthetic model is the ability to choose the object placement distribution (Griffiths & Boehm, 2019). In addition, the synthetic point clouds do not present occlusions, but the realism of the urban scene is lost. In SUD dataset, the creation of synthetic data was not performed as the streets were scanned with MLS and HMLS systems and many of the occlusions were corrected by combining both data. Besides, it is intended that in the future this dataset will be used for urban mobility studies, and not only to evaluate semantic segmentation algorithms.

Table 1 compares the characteristics of some of the 3D point clouds datasets, sorted chronologically, available in outdoor environment.

3. Dataset generation

3.1. Equipment

Point clouds were obtained with an MLS and a HMLS scanners. A Riegl VUX-1HA MLS scanner was used to acquire the point clouds from a car perspective. The most common mobile LiDAR system configuration integrates digital frame cameras, laser scanner, GNSS receiver, inertial navigation system (INS) for acceleration and orientation measurements of the moving platform, and a wheel-mounted Distance Measuring Indicator (DMI), that provides accurate vehicle velocity updates (Puente et al., 2011). The positioning sensors are vehicle-oriented to determine the absolute locations of the mobile mapping platform with respect to a global coordinate system. During the data acquisition, the GNSS/INS system calculates the trajectory and records the triggering events from the laser scanner inputs while the laser scanner measures two-dimensional points. Profile data is converted into three dimensions in the georeferencing phase where each of the laser points are assigned an appropriate time stamp and coupled with the trajectory information of the scanner's location and altitude.

The HMLS ZEB GO scanner was also used to scan the urban environment from a pedestrian perspective. The ZEB GO consists of a 2D time-of-flight laser range scanner rigidly coupled to an inertial measurement unit (IMU) mounted on a motor drive. The motion of the

Table 1
Comparison of urban point cloud datasets.

Dataset (Year)	World	RGB	Intensity	Length	N° points	Classes	LiDAR Sensor
Oakland (Munoz et al., 2009)	Real	No	No	1510 m	1.3 M	5	SICK LMS
Paris-rue-Madame (Serna et al., 2014)	Real	No	Yes	160 m	20 M	17	MLS system L3D2
iQumulus (Vallet et al., 2015)	Real	No	Yes	10000 m	300 M	11	MLS system Stereopolis II
Semantic3D (Hackel et al., 2017)	Real	Yes	Yes	4500 m	4009 M	9	Terrestrial Laser Scanner
Paris-Lille-3D (Roynard et al., 2018)	Real	No	Yes	1940 m	143 M	50	Velodyne HDL-32E
SynthCity (Griffiths & Boehm, 2019)	Synthetic	Yes	No	4000 *m*	368 M	9	Blender 3D graphics software
Toronto-3D (Tan et al., 2020)	Real	Yes	Yes	1000 m	78 M	9	MLS Teledyne Optech Maverick
TUM-MLS-2016 (Zhu et al., 2020)	Real	No	Yes	1000 m	41 M	9	Velodyne HDL-64E LiDAR
Paris-CARLA-3D (Deschaud et al., 2021)	Synthetic + Real	Yes	Yes (Synthetic) No (Real)	550 m + 5800 m	700 + 60 M	23	CARLA Simulator + LiDAR Velodyne HDL32
SUD (Ours)	**Real**	**No**	**Yes (MLS) No (HMLS)**	**1635 m (MLS) 2089 m (HMLS)**	**296 M (MLS) 167 M (HMLS)**	**8**	**MLS Riegl VUX-1HA + HMLS Zeb GO**

scanning head on the motor drive provides the third dimension required to generate 3D information. A novel 3D simultaneous localization and mapping algorithm is used to combine the 2D laser scan data with the IMU data to generate accurate 3D point clouds. The ZEB GO captures raw laser range measurement and inertial data. Then, this data must be processed using GeoSLAM's algorithm to convert the raw data into a 3D point cloud using the GeoSLAM Hub processing application (Geoslam, 2022).

Table 2 shows the technical characteristics of Riegl VUX-1HA (RIEGL Laser Measurement Systems GmbH, 2022) and ZEB-GO (Geoslam, 2022) systems.

3.2. Scanned area

The survey was conducted in Santiago de Compostela (Spain), in February 2022. The dataset contains fourteen segments of six urban streets. Each segment measures approximately 200 m, therefore the dataset is formed by 1.6 km MLS point clouds and 2 km HMLS point clouds of urban streets (Fig. 1). The República Argentina Street (segments A, B and C) was acquired with the HMLS system, and only 50 m of this street (section of segment A) were acquired with the MLS system.

3.3. Point cloud registration

Point clouds obtained with the ZEB-GO laser scanner are not georeferenced, therefore, HMLS point clouds were registered with respect to the MLS point clouds with CloudCompare (CloudCompare, 2022). To do an accurate registration, at least four points were selected in corners of the MLS point clouds and their counterparts in the HMLS point cloud. Table 3 shows the number of meters, points and the registration error of each segment. Registration error was directly obtained from the CloudCompare registration tool. República Argentina street was registered regarding GPS points due to this street was not scanned with the Riegl system. Therefore, the registration error in segments A, B and C is higher.

3.4. Labelling

The workflow to label MLS and HMLS point clouds is shown in Fig. 2. Manual labelling was conducted with CloudCompare, that was combined with automatic processes to reduce the human effort. The following rules were established to obtain uniform and consistent labelling:

- All the points behind the facade line were considered as *building* points, including flooring of entrances, doors, shop windows, etc.
- Only stationary cars and vans were considered as *vehicles*.
- Motorbikes, large trucks, or any vehicle in movement were classified as class *others*.
- Any element in the ground space that is neither trees nor stationary cars/trucks was classified as *others*.

First, 200 m of MLS point cloud data were manually labelled in five classes (*ground*, *building*, *vehicles*, *vegetation* and *others*). These first 200 m labelled data was used to train PointNet++ (Qi et al., 2017), and implement a preliminary classification of the remaining point clouds. The point clouds classified by PointNet++ had only a 0.75 of accuracy, but they were a great help for supporting subsequent manual labelling.

After obtaining all the segments classified in five classes, k-Nearest Neighbours (KNN) algorithm (S. Zhang et al., 2018) was applied to the HMLS data to assign labels by proximity from MLS data. For each point in the HMLS point cloud, the nearest neighbour in the MLS point cloud is located, and subsequently, the class of the MLS point is assigned to the corresponding HMLS point. However, some points were misclassified; for example, cars in different positions between MLS and HMLS scans. Therefore, a manual correction was done to correct the remaining misclassified points.

After obtaining the MLS and HMLS point clouds labelled into five classes, the *ground* was split into *road*, *sidewalk* and *curb*. Following a similar process as (Balado Frias et al., 2017), an algorithm was applied to the ground points of the MLS data in order to separate the vertical ground elements (*curbs*) from de horizontal ones (*sidewalks* and *road*), using the values of inclination, curvature and DBSCAN algorithm (Wang et al., 2019). Then, the horizontal elements were manually separated into *sidewalk* and *road*. The ground points of the HMLS data were classified applying a KNN algorithm, referring to the classified ground points of the MLS data. Some points were misclassified due to the occlusions in the MLS data, therefore ground points of the HMLS data had to be manually corrected.

From the class *others*, the class *pole-likes* were extracted. DBSCAN algorithm was applied to individualize the class *others* of the MLS point clouds. *Pole-like elements* were obtained filtering by height and width. The class *others* of the HMLS data was classified into *pole-like elements* and *others* with a KNN algorithm, referring to the classified data *others* of the MLS data. Again, some corrections were done. Finally, both MLS and HMLS data were classified into 8 classes: *road*, *sidewalk*, *curb*, *building*, *vehicles*, *vegetation*, *pole-like elements* and *others* (Fig. 3 and Fig. 4).

Tables 4 and 5 show the number of meters, the total number of points and the number of points per class in each street, regarding MLS data and HMLS data respectively. The values of number of meters, points and points per class of the dataset are also represented for both types of data. The labelling process was optimized, however, around 600 h of manual classification were required.

4. Baseline

4.1. Neural network

PointNet++ model was tested on the proposed dataset as baseline approach. This architecture is commonly used in Deep Learning applications with point clouds (Garcia-Garcia et al., 2016; Z. Zhang et al., 2020). The operation of PointNet++ is based on the following steps. First the set of points is partitioned into overlapping local regions. The local features are extracted from small neighbourhoods; such local features are further grouped into larger units and processed to produce higher level of features until the features of the whole point set are obtained.

The model was trained and tested on a GPU NVIDIA A100 Tensor Core with 40G of RAM. Table 6 compiles the parameters used for the pre-processing and training of PointNet++. Different pre-processing steps and training parameters were tested to find the best configuration for the specific dataset. The number of epochs and the batch size were chosen based on metrics obtained with different test, varying both parameters. The cube size was chosen regarding memory restrictions and the number of points was selected searching a compromise with the cube size.

4.2. Implementation

Given the existence of two data sources, three tests with their corresponding three training sessions were performed: one with only MLS

Table 2
Technical characteristics of Riegl VUX-1HA and ZEB-GO.

	Riegl VUX-1HA	ZEB-GO
Field of view (vertical/horizontal)	360° full circle	270°/360°
Angular resolution (vertical/horizontal)	0.001°	1.8°/0.625°
Range (m)	1.2–420	30
Accuracy (mm)	5	10–30
Pts/s	Up to 1,000,000	43,200
Wavelength (nm)	Near infrared	905
Weight (kg)	3.75	1

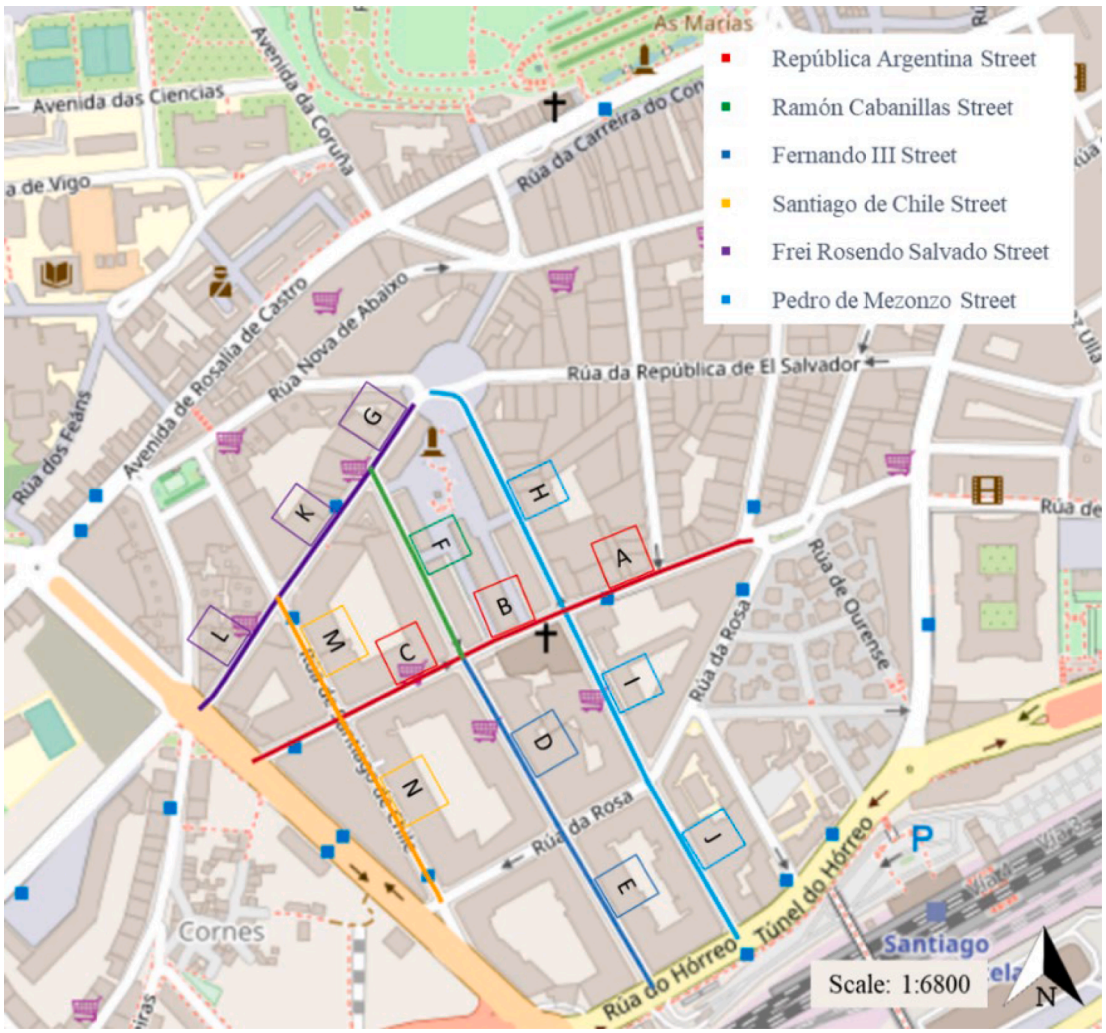

Fig. 1. Scanned urban area. The visualization of the streets is overlaid on an OpenSteetMaps map.

Table 3
Characteristics of HMLS data.

HMLS data				
Street	**Segment**	**Length (m)**	**Num. points**	**Registration error (m)**
República Argentina*	A	161.0	13,724,766	0.47
	B	94.5	8,717,573	0.67
	C	188.8	16,896,888	0.72
Ramón Cabanillas	F	179.1	13,163,458	0.18
Fernando III	D	167.4	13,183,486	0.098
	E	147.8	11,016,596	0.08
Santiago de Chile	M	123.0	10,262,331	0.17
	N	201.0	16,071,852	0.17
Frei Rosendo Salvado	L	107.9	9,605,623	0.028
	G	76.3	5,283,901	0.044
	K	150.2	6,026,889	0.029
Pedro Mezonzo	H	195.1	17,966,453	0.069
	I	149.8	12,356,344	0.056
	J	147.3	13,050,813	0.084

*República Argentina street was registered regarding GPS points due to this street was not scanned with the Riegl system.

point clouds, another one with only HMLS point clouds and a third one using both MLS and HMLS point clouds. The dataset was divided into training, validation, and test sets. For validation and testing, 200 m segments with overlap between MLS and HMLS data were selected. In addition, validation and test sets were checked for the absence of elements do not present in the training dataset. Segments I and K segments were selected for validation and segments F and M were selected for test (Fig. 5).

4.3. Metrics

To assess the model's performance, several metrics were employed, including confusion matrices, precision, recall, F1-score, intersection over union (IoU) for each class, and the mean IoU. Precision measures the ratio of correctly predicted positive observations to the total predicted positive observations (Equation (1), with TP representing true positive values and FP representing false positive values. Recall, on the other hand, calculates the ratio of correctly predicted positive observations to all observations in the actual class (Equation (2), with FN representing false negative values. The F1-Score, being the weighted average of precision and recall, takes into account both false positives (FP) and false negatives (FN) (Equation (3). For evaluating the performance of each class, IoU (Equation (4) is employed, where *i* denotes the class. Lastly, the mean IoU (Equation (5) provides an overall assessment of the semantic segmentation's quality.

$$Precision = \frac{TP}{TP + FP} \tag{1}$$

$$Recall = \frac{TP}{TP + FN} \tag{2}$$

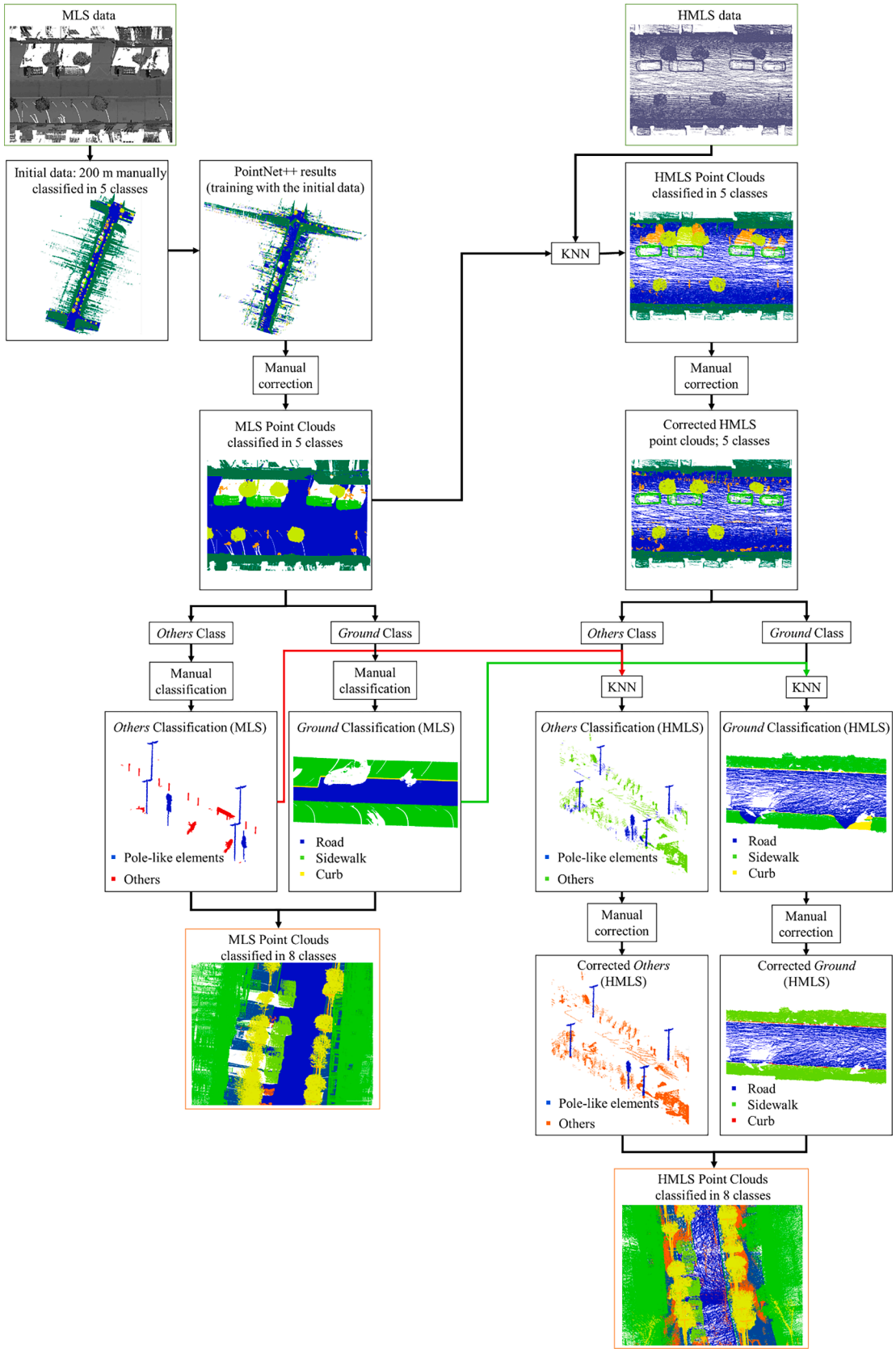

Fig. 2. Labelling workflow. Green squares represent the input data and orange squares the final labelled data. (For interpretation of the references to colour in this figure legend, the reader is referred to the web version of this article.)

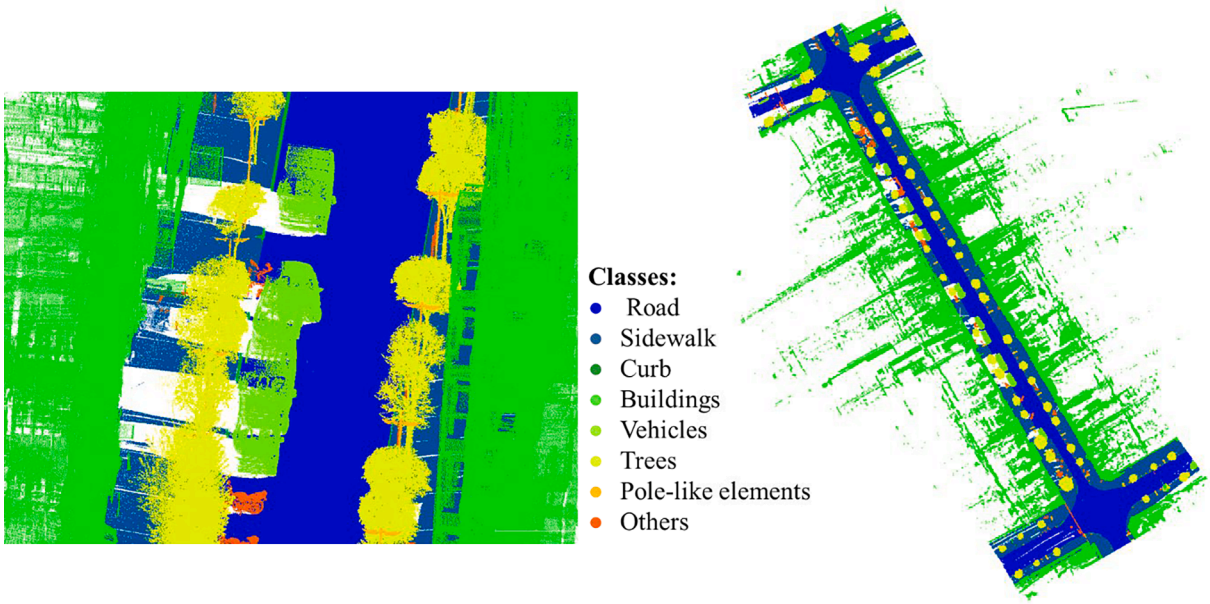

Fig. 3. MLS data classification into 8 classes.

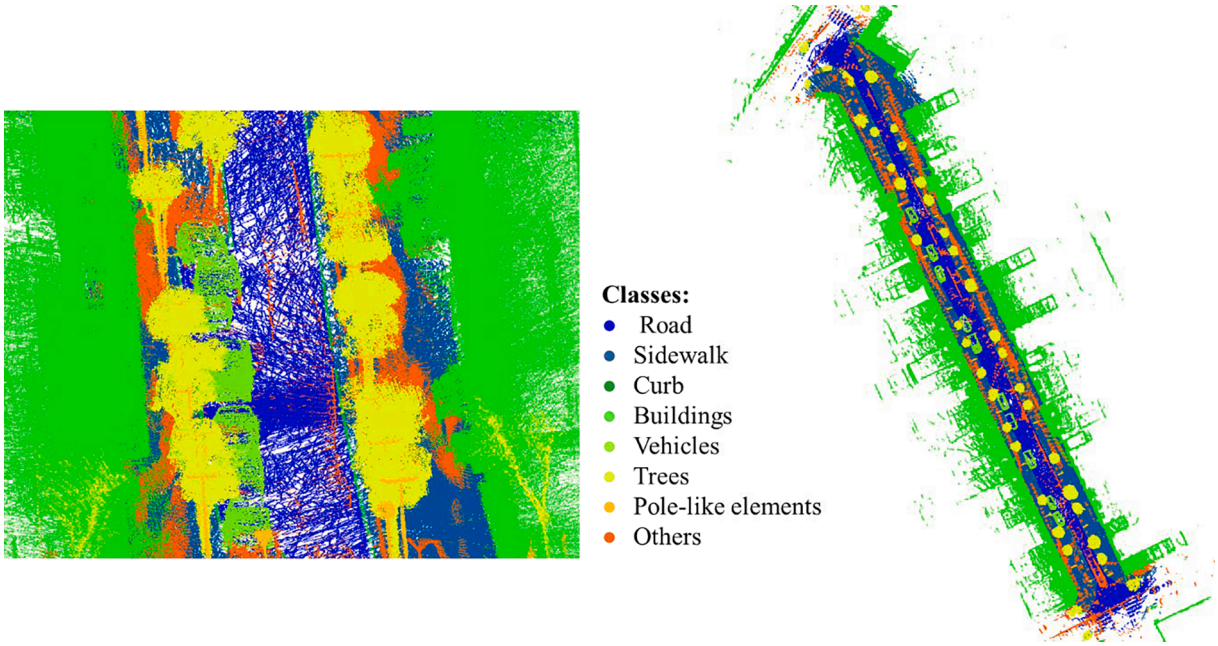

Fig. 4. HMLS data classification into 8 classes.

$$F1\_score = 2^{*}\frac{Precsion^{*}Recall}{Precision + Recall} \tag{3}$$

$$IoU_i = \frac{TP_i}{TP_i + FP_i + FN_i} \tag{4}$$

$$\overline{IoU} = \frac{1}{N}\sum_{i=1}^{N} IoU_i \tag{5}$$

4.4. Results

Table 7, Table 8 and Table 9 show the confusion matrices considering MLS data, HMLS data and H&MLS data respectively. Results of the abovementioned metrics are compiled in Table 10 for MLS data, Table 11 for HMLS and Table 12 for MLS and HMLS.

The behaviour of PointNet++ in the predictions was as expected. The best identified classes were those corresponding to the largest number of points and distinctive geometries (*road, sidewalk, buildings, vehicles,* and *vegetation*). Likewise, the *ground* class did not achieve as high hit rates as in other works (Tan et al., 2020) because it was divided into three classes (*road, sidewalks* and *curbs*). It is also worth noting that the classification with MLS data is better than with HMLS, which may be justified by the lower quality of the HMLS point cloud (less point density and less precision). On the other hand, it is interesting to check how the union of MLS and HMLS does not improve the classification. Future works will study this behaviour in more detail. Fig. 6 shows the results obtained with the three models in the test data.

Table 4
Number of points and meters scanned with MLS per street.

MLS data Street	Street meters	Total num. of points	Num. of points per class							
			Road	Sidewalk	Curb	Buildings	Vehicles	Trees	Pole-like	Others
República Argentina	52.7	11,113,830	1,979,064	1,042,534	105,775	7,392,622	213,058	290,902	50,801	39,074
Ramón Cabanillas	178.12	30,828,846	5,305,175	4,603,088	249,264	17,416,993	872,227	1,903,385	182,027	296,687
Fernando III	333.1	49,606,416	9,407,063	6,391,132	368,079	29,155,235	814,850	2,368,449	281,236	820,372
Santiago de Chile	299.7	68,719,549	14,627,929	3,021,162	173,614	43,923,460	5,047,461	889,251	196,218	840,454
Frei Rosendo Salvado	313.1	60,811,417	11,198,283	7,358,812	676,678	36,392,723	984,493	2,442,067	282,136	1,476,225
Pedro Mezonzo	458.7	75,162,564	15,114,656	8,026,624	594,869	41,947,838	3,070,328	3,981,101	374,977	2,052,171
Total	**1635.4**	**296,242,622**	**5,763,2170**	**30,443,352**	**2,168,279**	**176,228,871**	**11,002,417**	**11,875,155**	**1,367,395**	**5,524,983**

Table 5
Number of points and meters scanned with HMLS per street.

HMLS data Street	Street meters	Total num. of points	Num. of points per class							
			Road	Sidewalk	Curb	Buildings	Vehicles	Trees	Pole-like	Others
República Argentina	444.3	39,339,227	4,577,460	8,087,385	—	21,543,974	1,343,479	1,095,806	344,572	2,346,551
Ramón Cabanillas	179.1	13,163,458	765,371	4,177,145	37,011	6,451,801	236,267	756,051	120,046	619,766
Fernando III	315.2	24,200,082	1,875,792	6,350,938	74,223	12,938,420	487,683	1,182,827	214,424	1,075,775
Santiago de Chile	324.0	26,334,183	3,145,861	5,012,419	148,260	14,743,982	1,320,996	460,214	245,358	1,257,093
Frei Rosendo Salvado	334.4	20,916,413	1,216,984	5,014,617	105,643	12,518,601	151,194	595,940	134,061	1,179,373
Pedro Mezonzo	492.2	43,373,610	2,951,666	11,603,368	270,998	22,765,308	1,731,343	2,053,345	337,661	1,659,921
Total	**2089.2**	**167,326,973**	**14,533,134**	**40,245,872**	**636,135**	**90,962,086**	**5,270,962**	**6,144,183**	**1,396,122**	**8,138,479**

Table 6
PointNet ++: Pre-processing and training parameters.

Random Cubes size	10 m per point cloud
Random Rotation	Z axis
Random sampling	32,768 points
Scale data	[0,1]
Epochs	2000
Batch size	2
Optimizer	Adam
Learning Rate	0.001
Batch normalization momentum	0.9

5. Discussion and improvements

The main contribution of this research is the generation of a labelled urban dataset with the ground classified into *road*, *sidewalk* and *curbs,* and combining H&MLS data in order to reduce the occlusions caused by parked cars or street furniture.

Data labelling poses a significant challenge in the pursuit of acquiring a meticulously annotated dataset. In (Deschaud et al., 2021), the data labelling endeavour was executed exclusively through manual means using the software CloudCompare, engaging the participation of three individuals across three distinct phases, to annotate the point clouds. Similarly, within the context of the present method, a concerted effort was made to integrate automated labelling techniques. However, the data labelling process necessitated a significant reliance on manual

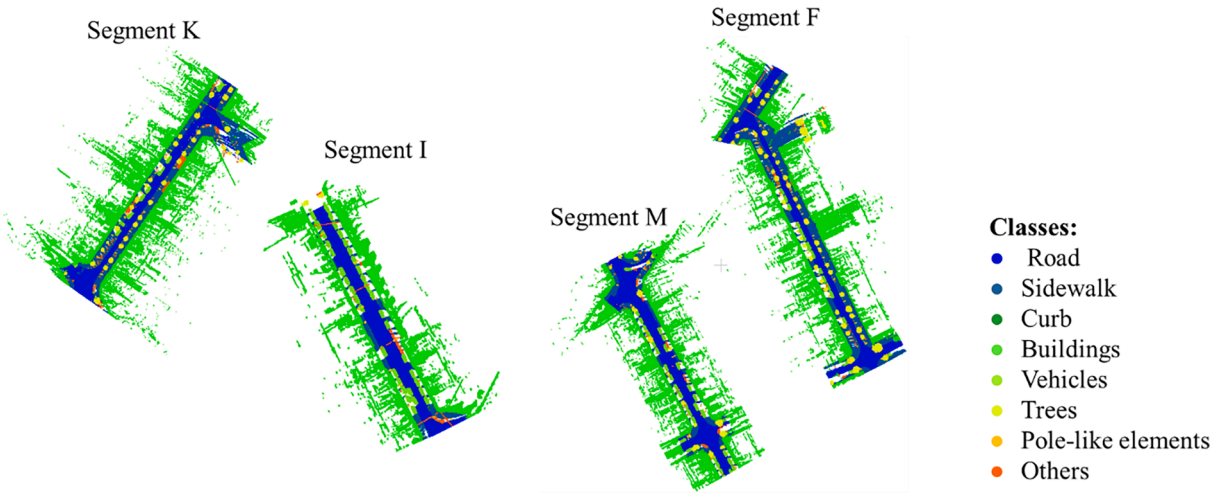

Fig. 5. Deep Learning model data: validation and test data.

Table 7
Confusion Matrix: MLS data.

Ref/Pred	Road	Sidewalk	Curb	Building	Vehicles	Vegetation	Poles	Others
Road	666,849	6845	2493	1345	221	0	0	301
Sidewalk	66,183	310,136	4451	6132	881	202	98	5245
Curb	3045	1887	14,261	138	206	3	0	146
Building	51,562	104,647	2796	3,578,057	9239	67,912	12,059	117,968
Vehicles	2187	451	147	2056	101,364	38	249	22,806
Vegetation	38	327	88	1029	14	170,023	1011	4030
Poles	7	409	37	446	0	3223	13,659	761
Others	483	2626	509	3353	2678	860	2226	24,920

Table 8
Confusion Matrix: HMLS data.

Ref/Pred	Road	Sidewalk	Curb	Building	Vehicles	Vegetation	Poles	Others
Road	242,419	6879	0	912	1262	2	1	230
Sidewalk	253,953	401,296	0	9001	610	111	181	243
Curb	7224	2050	0	60	90	0	1	9
Building	11,733	60,703	0	1,481,454	1284	26,344	2552	15,579
Vehicles	3236	301	0	1248	53,603	44	111	2706
Vegetation	1739	224	0	2126	5634	91,861	2211	1091
Poles	197	42	0	2697	495	6337	19,091	2081
Others	7244	4617	0	23,282	43,507	4271	6746	59,717

Table 9
Confusion Matrix: H&MLS data.

Ref/Pred	Road	Sidewalk	Curb	Building	Vehicles	Vegetation	Poles	Others
Road	601,546	16,486	3939	6159	1296	0	0	280
Sidewalk	126,572	355,864	10,333	34,260	551	184	47	1865
Curb	6385	4454	5950	367	336	1	1	105
Building	42,324	63,692	337	3,702,201	14,519	32,547	21,304	43,855
Vehicles	2766	167	98	8823	115,991	21	0	3989
Vegetation	233	491	204	13,335	515	168,266	1776	5860
Poles	6	423	28	1454	186	3987	16,445	2029
Others	2455	3691	725	12,629	14,623	1850	951	38,897

Table 10
Metric results (MLS data).

	Road	Sidewalk	Curb	Building	Vehicles	Vegetation	Poles	Others
Precision	0.8437	0.7258	0.5755	0.9960	0.8845	0.7018	0.4661	0.1414
Recall	0.9835	0.7885	0.7244	0.9072	0.7840	0.9630	0.7367	0.6618
F1-Score	0.9083	0.7558	0.6414	0.9495	0.8312	0.8119	0.5710	0.2331
IoU	0.8319	0.6075	0.4721	0.9038	0.7111	0.6834	0.3996	0.1319
$\overline{IoU}$				0.8186				

Table 11
Metric results (HMLS data).

	Road	Sidewalk	Curb	Building	Vehicles	Vegetation	Poles	Others
Precision	0.4593	0.8429	0.0000	0.9741	0.5034	0.7123	0.6180	0.7313
Recall	0.9631	0.6031	0.0000	0.9261	0.8752	0.8758	0.6170	0.3998
F1-Score	0.6220	0.7031	0.0000	0.9495	0.6391	0.7856	0.6175	0.5169
IoU	0.4514	0.5421	0.0000	0.9039	0.4697	0.6469	0.4466	0.3486
$\overline{IoU}$				0.6575				

Table 12
Metric results (H&MLS data).

	Road	Sidewalk	Curb	Building	Vehicles	Vegetation	Poles	Others
Precision	0.7690	0.7992	0.2753	0.9796	0.7836	0.8134	0.4058	0.4015
Recall	0.9553	0.6719	0.3381	0.9443	0.8797	0.8825	0.6696	0.5130
F1-Score	0.8521	0.7300	0.3035	0.9616	0.8289	0.8465	0.5054	0.4505
IoU	0.7422	0.5748	0.1789	0.9261	0.7078	0.7339	0.3381	0.2907
$\overline{IoU}$				0.7318				

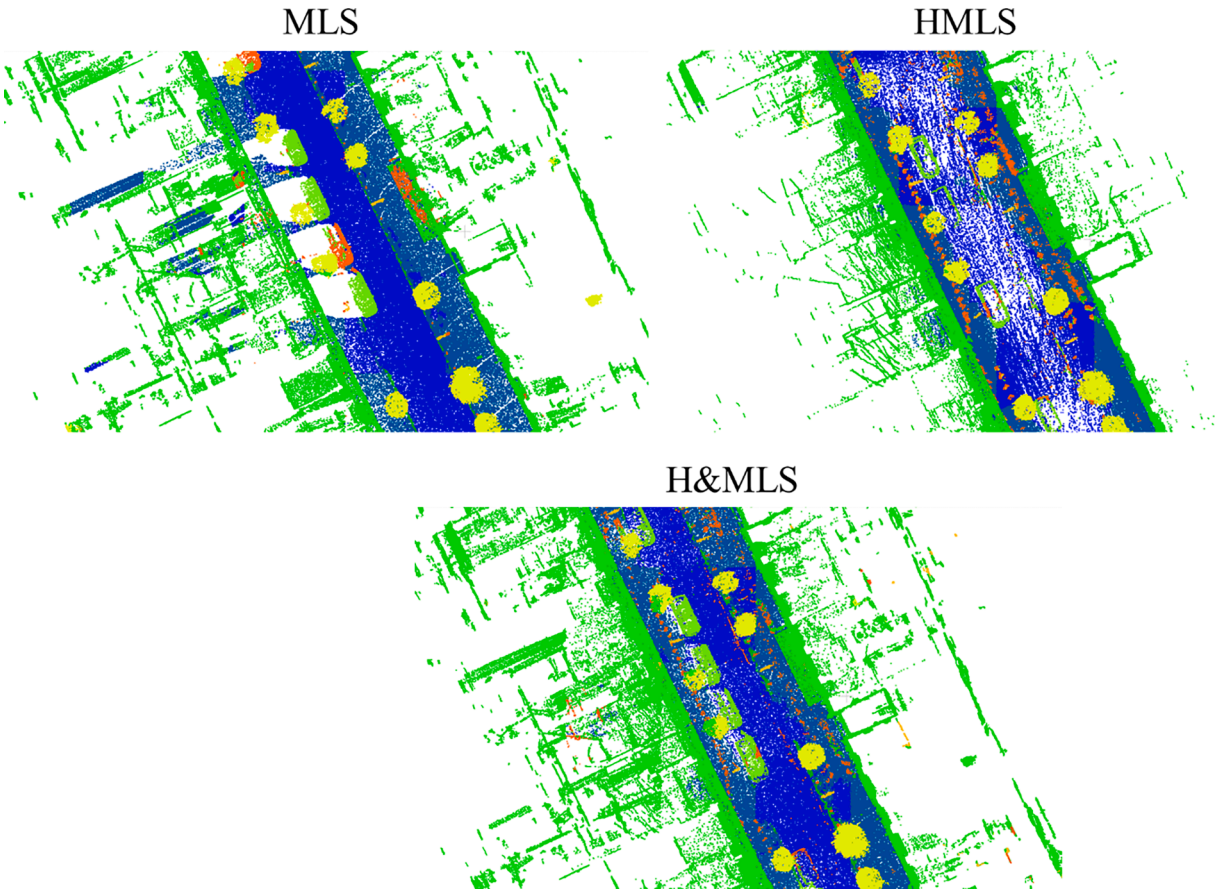

Fig. 6. Zoom in segment D. MLS, HMLS and H&MLS Deep Learning results.

intervention, highlighting the continued importance of human expertise and oversight in achieving accurate annotations. In the present method, six individuals labelled the point clouds using the software CloudCompare. Although initial attempts using Machine Learning and Deep Learning models were undertaken for segmentation, the achieved classification did not meet the requisite quality standards for final publication. Consequently, an alternative approach was adopted, involving the initial application of PointNet++ for semantic segmentation on MLS (Mobile Laser Scanning) data, but with a reduced set of classes. This preliminary segmentation served as a visual aid, facilitating subsequent manual correction to enhance accuracy.

Furthermore, established heuristic algorithms were implemented to segment and classify the dataset into the eventual eight classes. Meanwhile, considering the availability of two distinct data sources, a similar process was contemplated for the HMLS (Handheld Mobile Laser Scanning) data. However, due to the inferior classification outcomes compared to the MLS data, a point-to-point class assignment method based on the K-Nearest Neighbors (KNN) technique was selected. This approach allowed for the identification of errors with relative ease in the classification process.

The incorporation of HMLS data played a crucial role in addressing occlusions within the urban scene, allowing PointNet++ to accurately classify points located within these occluded areas (as depicted in Fig. 6). This outcome proved elusive when attempting label assignments solely based on proximity to the MLS (Mobile Laser Scanning) point cloud. However, the contribution of HMLS data was not uniformly distributed across the entire environment. While both sides of vehicles were thoroughly surveyed, one using MLS and the opposite using HMLS, the representation of curbs in the HMLS point cloud was less comprehensive. This limitation arises from the methodology employed, as the perspective from the sidewalk was utilized while moving with the ZEB-GO system. Consequently, the number of curb points acquired using the ZEB-GO device was notably lower when compared to the Riegl system, as clearly depicted in Table 4 and Table 5.

Furthermore, it is important to note that the quality of the HMLS point cloud fell short of that achieved by the MLS point cloud. The HMLS data required manual registration in relation to the MLS point clouds. Consequently, georeferenced HMLS point clouds exhibited registration errors, with magnitudes ranging from 0.03 to 0.1 m. It is worth highlighting that the República Argentina street data displayed a more significant registration error due to the utilization of GPS points, leading to a reduction in the precision of the registration process. These registration errors were notably influenced by the deformation observed in the point clouds acquired through the ZEB-GO system. Several scans were deemed unusable due to inaccurate SLAM (Simultaneous Localization and Mapping) performance, particularly in cases where objects displayed displacements of up to 1 m near the start and end of the scan. This phenomenon was particularly pronounced in areas featuring highly repetitive patterns on building façades. A potential solution for the future might involve the implementation of nonrigid ICP (Cheng et al., 2015). However, tests indicated that such nonrigid ICP algorithms come with significant computational demands, especially when dealing with large point clouds.

The acquisition of ZEB-GO data was strategically planned to accommodate the inherent limitations of the scanner. The survey area was subdivided into individual scans, each of which was carefully designed to span no more than 15 min in duration. Additionally, the scanning trajectory for each instance of the ZEB-GO was meticulously charted in a pattern resembling the numeral “eight,” with both the initiation and conclusion points of the trajectory coinciding at the same geographical location (as illustrated in Fig. 7).

When assessing the performance of the trained models by comparing

F1-score and IoU values, all models exhibited high-quality results. Specifically, the obtained mean IoU values consistently exceeded 0.65, further solidifying the efficacy of PointNet++ and establishing the validity of the dataset for the evaluation of alternative semantic segmentation algorithms. In a parallel examination of datasets that incorporate both real and synthetic point clouds, (Deschaud et al., 2021) similarly utilized the PointNet++ architecture as one classification methodology. However, their investigation yielded an aggregate IoU of merely 0.14. Intriguingly, their results indicated a discernible performance disparity, wherein the employment of the PointNet++ architecture exhibited superior outcomes when applied to real point clouds as opposed to synthetic point clouds. This contrast underscores the nuanced intricacies inherent in the utilization of such architectures across divergent data sources.

It is noteworthy that all classes within the dataset are accurately represented, maintaining a distribution of point counts that mirrors a realistic scenario. Nevertheless, a recurring observation, consistent with findings in related research (Deschaud et al., 2021), reveals that most elements lack precise delineation, leading to significant confusion, particularly in areas adjacent to one another (as illustrated in Fig. 6).

Furthermore, both the labelled and predicted data demonstrate a high degree of utility for the examination of urban mobility, encompassing both pedestrian and vehicular aspects. Moreover, the dataset's completeness and extensive coverage make it a valuable resource for investigations in the fields of urban planning and geometry. This multifaceted utility is a direct consequence of the comprehensive nature of the survey.

6. Conclusion

This study introduced a new urban point cloud dataset, known as the Santiago Urban Dataset (SUD). SUD was meticulously labelled with eight distinct classes, including *road, sidewalk, curb, buildings, vehicles, vegetation, poles*, and a category denoted as *others*. Notably, SUD dataset is a composite dataset, merging Handheld Mobile Laser Scanning (HMLS) and Mobile Laser Scanning (MLS) point clouds. One of the key advancements achieved in this work was the utilization of data fusion techniques to effectively handle occlusions introduced by parked vehicles and furniture. This approach mitigated the challenges posed by these occlusions, thereby enhancing the overall quality of urban point cloud data.

The PointNet++ model was selected as a baseline approach for evaluation, and several pertinent metrics were introduced to assess its performance. The outcomes of this evaluation were notably consistent with those observed in other state-of-the-art works. Both the quantity and spatial distribution of errors align with established benchmarks, affirming that the SUD dataset is well-suited for comparative assessments of new Deep Learning models targeting semantic segmentation tasks. Beyond its applicability in model comparisons, the broad scope of the survey, coupled with the integration of HMLS and MLS data, significantly extends the potential applications of the SUD. This dataset can serve as a valuable resource for studies spanning urban mobility, urban planning, functional spatial analysis, and investigations into urban geometry. This multifaceted utility is a direct result of the extensive data coverage and the inclusion of data from both HMLS and MLS sources.

As future work, other Deep Learning models will be tested on the dataset as well as new architectures. Different frameworks to integrate and fusion HMLS data into MLS data will also be studied. The SUD is free and public on Github (González-Collazo, 2022).

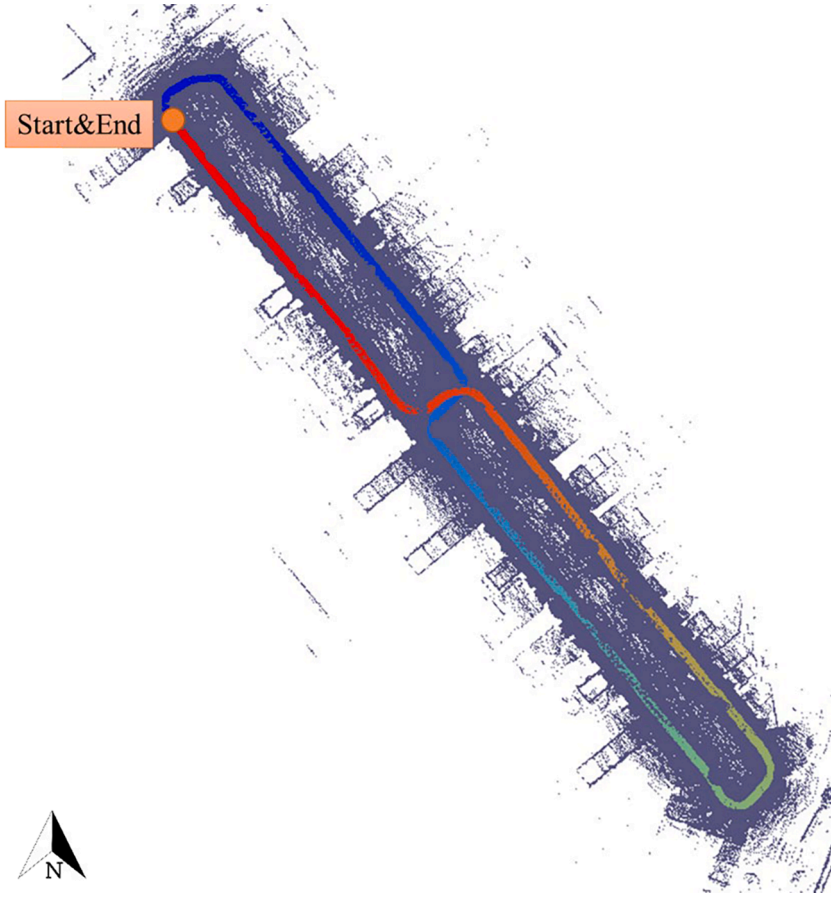

Fig. 7. Scanning trajectory with ZEB GO (multicolor line).

CRediT authorship contribution statement

Silvia María González-Collazo: Methodology, Software, Writing – original draft, Writing – review & editing. **Jesús Balado:** Conceptualization, Methodology, Writing – review & editing, Supervision. **Iván Garrido:** Methodology, Software. **Javier Grandío:** Software. **Rabia Rashdi:** Resources. **Elisavet Tsiranidou:** Resources. **Pablo del Río-Barral:** Investigation, Resources. **Erik Rúa:** Investigation, Resources. **Iván Puente:** Investigation. **Henrique Lorenzo:** Project administration.

Declaration of Competing Interest

The authors declare that they have no known competing financial interests or personal relationships that could have appeared to influence the work reported in this paper.

Data availability

I have shared the dataset in the following link https://github.com/SilviaMGC/SUD-Dataset

Acknowledgements

This research was funded by the Xunta de Galicia, grant numbers ED481B-2019-061 and ED431C 2020/01, and by the Ministerio de Ciencia, Innovación y Universidades -Gobierno de España-, grant number PID2019-105221RB-C43/AEI/10.13039/501100011033. This paper was carried out in the framework of the InfraROB project (Maintaining integrity, performance and safety of the road infrastructure through autonomous robotized solutions and modularization), which has received funding from the European Union's Horizon 2020 research and innovation programme under grant agreement no. 955337. It reflects only the authors' views. Neither the European Climate, Infrastructure, and Environment Executive Agency (CINEA) nor the European Commission is in any way responsible for any use that may be made of the information it contains. Authors also would like to thank to CESGA for the use of their servers. Funding for open access charge: Universidade de Vigo/CISUG.

References

Balado Frias, J., Díaz Vilariño, L., Arias, P., & Garrido, I. (2017). Point clouds to indoor/outdoor accessibility diagnosis. *ISPRS Annals of Photogrammetry, Remote Sensing and Spatial Information Sciences, IV-2/W4*, 287–293. https://doi.org/10.5194/isprs-annals-IV-2-W4-287-2017

Balado, J., Díaz-Vilariño, L., Arias, P., & Lorenzo, H. (2019). Point clouds for direct pedestrian pathfinding in urban environments. *ISPRS Journal of Photogrammetry and Remote Sensing, 148*, 184–196. https://doi.org/10.1016/j.isprsjprs.2019.01.004

Barros-Ribademar, J., Balado, J., Arias, P., & González-Collazo, S. M. (2022). Visibility analysis for the occlusion detection and characterisation in street point clouds acquired with Mobile Laser Scanning. *Geocarto International*, 1–18. https://doi.org/10.1080/10106049.2022.2032392

Bello, S. A., Yu, S., Wang, C., Adam, J. M., & Li, J. (2020). Review: Deep learning on 3D point clouds. *Remote Sensing, 12*(11). https://doi.org/10.3390/rs12111729

Chang, A., Dai, A., Funkhouser, T., Halber, M., Nießner, M., Savva, M., Song, S., Zeng, A., & Zhang, Y. (2017). *Matterport3D: Learning from RGB-D Data in Indoor Environments*.

Cheng, S., Marras, I., Zafeiriou, S., & Pantic, M. (2015). *Active nonrigid ICP algorithm*. 10.1109/FG.2015.7163161.

CloudCompare. (2022). *CloudCompare*. https://www.cloudcompare.org/main.html.

Dai, A., Chang, A., Savva, M., Halber, M., Funkhouser, T., & Nießner, M. (2017). *ScanNet: Richly-annotated 3D Reconstructions of Indoor Scenes*.

Deschaud, J.-E., Duque, D., Richa, J. P., Velasco-Forero, S., Marcotegui, B., & Goulette, F. (2021). Paris-CARLA-3D: A real and synthetic outdoor point cloud dataset for challenging tasks in 3D mapping. *Remote Sensing, 13*(22). https://doi.org/10.3390/rs13224713

Fernandes, D., Silva, A., Névoa, R., Simões, C., Gonzalez, D., Guevara, M., … Melo-Pinto, P. (2021). Point-cloud based 3D object detection and classification methods for self-driving applications: A survey and taxonomy. *Information Fusion, 68*, 161–191. https://doi.org/10.1016/j.inffus.2020.11.002

Fernández-Arango, D., Varela-García, F.-A., González-Aguilera, D., & Lagüela-López, S. (2022). Automatic generation of urban road 3D models for pedestrian studies from LiDAR data. *Remote Sensing, 14*(5). https://doi.org/10.3390/rs14051102

Gao, X., Wang, Q., Gu, H., Zhang, F., Peng, G., Si, Y., & Li, X. (2021). Fully automatic large-scale point cloud mapping for low-speed self-driving vehicles in unstructured environments. *IEEE Intelligent Vehicles Symposium (IV), 2021*, 881–888. https://doi.org/10.1109/IV48863.2021.9575571

Garcia-Garcia, A., Gomez-Donoso, F., Garcia-Rodriguez, J., Orts-Escolano, S., Cazorla, M., & Azorin-Lopez, J. (2016). PointNet: A 3D Convolutional Neural Network for real-time object class recognition. *2016 International Joint Conference on Neural Networks (IJCNN)*, 1578–1584. 10.1109/IJCNN.2016.7727386.

Geoslam. (2022). *GeoSLAM*. https://geoslam.com/wp-content/uploads/2021/02/ZEB_Go_User_Guide_1.0.7.pdf.

González-Collazo, S. M. (2022). *SUD Dataset*. https://github.com/SilviaMGC/SUD-Dataset.

Gouda, M., Mirza, J., Weiß, J., Ribeiro Castro, A., & El-Basyouny, K. (2021). Octree-based point cloud simulation to assess the readiness of highway infrastructure for autonomous vehicles. *Computer-Aided Civil and Infrastructure Engineering, 36*(7), 922–940. https://doi.org/10.1111/mice.12643

Griffiths, D., & Boehm, J. (2019). *SynthCity: A large scale synthetic point cloud*.

Guo, Y., Wang, H., Hu, Q., Liu, H., Liu, L., & Bennamoun, M. (2021). Deep learning for 3D point clouds: A survey. *IEEE Transactions on Pattern Analysis and Machine Intelligence, 43*(12), 4338–4364. https://doi.org/10.1109/TPAMI.2020.3005434

Hackel, T., Savinov, N., Ladicky, L., Wegner, J. D., Schindler, K., & Pollefeys, M. (2017). Semantic3D.net: A new Large-scale Point Cloud Classification Benchmark. *ArXiv, abs/1704.0*.

Ito, Y., & Takemura, K. (2021). Estimating Focused Pedestrian using Smooth-Pursuits Eye Movements and Point Cloud toward Assistive System for Wheelchair. *2021 IEEE International Conference on Systems, Man, and Cybernetics (SMC)*, 404–410. 10.1109/SMC52423.2021.9659153.

Justo, A., Soilán, M., Sánchez-Rodríguez, A., & Riveiro, B. (2021). Scan-to-BIM for the infrastructure domain: Generation of IFC-compliant models of road infrastructure assets and semantics using 3D point cloud data. *Automation in Construction, 127*, Article 103703. https://doi.org/10.1016/j.autcon.2021.103703

Kim, H., Yoon, J., & Sim, S.-H. (2020). Automated bridge component recognition from point clouds using deep learning. *Structural Control and Health Monitoring, 27*(9), e2591.

Liu, Z., van Oosterom, P., Balado, J., Swart, A., & Beers, B. (2022). Detection and reconstruction of static vehicle-related ground occlusions in point clouds from mobile laser scanning. *Automation in Construction, 141*, Article 104461. https://doi.org/10.1016/j.autcon.2022.104461

Ma, J. W., Czerniawski, T., & Leite, F. (2020). Semantic segmentation of point clouds of building interiors with deep learning: Augmenting training datasets with synthetic BIM-based point clouds. *Automation in Construction, 113*, Article 103144. https://doi.org/10.1016/j.autcon.2020.103144

Ma, W.-C., Tartavull, I., Bârsan, I. A., Wang, S., Bai, M., Mattyus, G., … Urtasun, R. (2019). Exploiting sparse semantic HD maps for self-driving vehicle localization. *IEEE/RSJ International Conference on Intelligent Robots and Systems (IROS), 2019*, 5304–5311. https://doi.org/10.1109/IROS40897.2019.8968122

Munoz, D., Bagnell, J. A., Vandapel, N., & Hebert, M. (2009). Contextual classification with functional Max-Margin Markov Networks. *IEEE Conference on Computer Vision and Pattern Recognition, 2009*, 975–982.

Murtiyoso, A., Veriandi, M., Suwardhi, D., Soeksmantono, B., & Harto, A. B. (2020). Automatic workflow for roof extraction and generation of 3D CityGML Models from low-cost UAV image-derived point clouds. *ISPRS International Journal of Geo-Information, 9*(12). https://doi.org/10.3390/ijgi9120743

Puente, I., Gonzalez, H., Arias, P., & Armesto, J. (2011). Land-based mobile laser scanning systems: A review. In *ISPRS Int Arch. of the Photogramm., Remote Sensing and Spatial Information Sciences*. https://doi.org/10.5194/isprsarchives-XXXVIII-5-W12-163-2011

Qi, C. R., Yi, L., Su, H., & Guibas, L. J. (2017). PointNet++: Deep hierarchical feature learning on point sets in a metric space. In I. Guyon, U. Von Luxburg, S. Bengio, H. Wallach, R. Fergus, S. Vishwanathan, & R. Garnett (Eds.), *Advances in neural information processing systems* (Vol. 30). Curran Associates Inc.

RIEGL Laser Measurement Systems GmbH. (2022). *Riegl*.

Romero-Jarén, R., & Arranz, J. J. (2021). Automatic segmentation and classification of BIM elements from point clouds. *Automation in Construction, 124*, Article 103576. https://doi.org/10.1016/j.autcon.2021.103576

Roynard, X., Deschaud, J.-E., & Goulette, F. (2018). Paris-Lille-3D: A Point Cloud Dataset for Urban Scene Segmentation and Classification. *2018 IEEE/CVF Conference on Computer Vision and Pattern Recognition Workshops (CVPRW)*, 2108–21083. 10.1109/CVPRW.2018.00272.

Serna, A., Marcotegui, B., Goulette, F., & Deschaud, J.-E. (2014). Paris-rue-Madame database: A 3D mobile laser scanner dataset for benchmarking urban detection, segmentation and classification methods. In *ICPRAM 2014 – Proceedings of the 3rd International Conference on Pattern Recognition Applications and Methods* (pp. 1–4).

Soilán, M., Riveiro, B., Sánchez-Rodríguez, A., & Arias, P. (2018). Safety assessment on pedestrian crossing environments using MLS data. *Accident Analysis and Prevention, 111*(December 2017), 328–337. 10.1016/j.aap.2017.12.009.

Soilán, M., Sánchez-Rodríguez, A., del Río-Barral, P., Perez-Collazo, C., Arias, P., & Riveiro, B. (2019). Review of laser scanning technologies and their applications for road and railway infrastructure monitoring. *Infrastructures, 4*(4). https://doi.org/10.3390/infrastructures4040058

Tan, W., Qin, N., Ma, L., Li, Y., Du, J., Cai, G., Yang, K., & Li, J. (2020). Toronto-3D: A Large-scale Mobile LiDAR Dataset for Semantic Segmentation of Urban Roadways. *2020 IEEE/CVF Conference on Computer Vision and Pattern Recognition Workshops (CVPRW)*, 797–806.

Vallet, B., Brédif, M., Serna, A., Marcotegui, B., & Paparoditis, N. (2015). TerraMobilita/iQmulus urban point cloud analysis benchmark. *Computers & Graphics, 49*, 126–133. https://doi.org/10.1016/j.cag.2015.03.004

Wang, C., Ji, M., Wang, J., Wen, W., Li, T., & Sun, Y. (2019). An improved DBSCAN method for LiDAR data segmentation with automatic eps estimation. *Sensors, 19*(1). https://doi.org/10.3390/s19010172

Zhang, S., Li, X., Zong, M., Zhu, X., & Wang, R. (2018). Efficient kNN classification with different numbers of nearest neighbors. *IEEE Transactions on Neural Networks and Learning Systems, 29*(5), 1774–1785. https://doi.org/10.1109/TNNLS.2017.2673241

Zhang, Z., Dai, Y., & Sun, J. (2020). Deep learning based point cloud registration: An overview. *Virtual Reality & Intelligent Hardware, 2*(3), 222–246. https://doi.org/10.1016/j.vrih.2020.05.002

Zhu, J., Gehrung, J., Huang, R., Borgmann, B., Sun, Z., Hoegner, L., … Stilla, U. (2020). TUM-MLS-2016: An annotated mobile LiDAR dataset of the TUM city campus for semantic point cloud interpretation in urban areas. *Remote Sensing, 12*(11). https://doi.org/10.3390/rs12111875

Zou, X., Cheng, M., Wang, C., Xia, Y., & Li, J. (2017). Tree classification in complex forest point clouds based on deep learning. *IEEE Geoscience and Remote Sensing Letters, 14*(12), 2360–2364. https://doi.org/10.1109/LGRS.2017.2764938